Cluster Characterization of 3D MIMO Propagation Channel in an Urban Macrocellular Environment

S. Sangodoyin, *Student Member, IEEE*, V. Kristem, *Student Member, IEEE*, C. U. Bas, *Student Member, IEEE*, M. Käske, J. Lee, *Senior Member, IEEE*, C. Schneider, G. Sommerkorn, J. Zhang, *Fellow, IEEE*, R. Thomä, *Fellow, IEEE*, and A. F. Molisch, *Fellow, IEEE*

***Abstract*—Multidimensional characterization of outdoor urban macrocellular propagation channels is essential for the analysis and design of next-generation (5G and beyond) cellular massive MIMO (Multiple-Input-Multiple-Output) systems. Since most massive MIMO arrays will extend in two or three dimensions, an understanding of three-dimensional (3D) parameters (i.e., azimuth and elevation) of the multipath components (MPCs) is required. This paper presents an extensive measurement campaign for 3D outdoor propagation channels in an urban macrocellular environment. Measurements were performed with a 20 MHz wideband polarimetric MIMO channel sounder centered at 2.53 GHz and MPCs were extracted using RIMAX – an iterative maximum likelihood (ML) algorithm. The physical propagation mechanisms of the observed discrete MPCs are explained in terms of waveguiding, over-the-rooftop propagation, and scattering by far-away objects. MPCs exhibit clustering in the temporal and spatial domains; both *intra-* and *inter-*cluster parameters and their relevant statistics are provided. We also extract diffuse MPCs, show that they can comprise a moderate portion of the overall energy, and provide a statistical characterization.**

***Index Terms*—Propagation channel, MIMO, clusters, multidimensional urban outdoor channel sounding, statistical channel model**

I. Introduction

INCREASING demand for higher data-rate services and the shortage of available spectrum has resulted in the pursuit of new ways to improve wireless communications infrastructure. To solve this challenge, a variety of techniques have been identified [2], [3], of which Massive MIMO (Multiple-Input-Multiple-Output) is a prominent one. The use of Massive MIMO [4], [5] in the form of Full-Dimensional MIMO (FD-MIMO) systems [6], [7], [8] is pursued, *inter alia*, by the Third Generation Partnership Project (3GPP) [9]. These systems utilize a large number of antennas placed on 3D antenna array panels[1] for realizing spatially distinct transmission links to a large number of mobile stations [4]. Due to the 3D nature of these arrays, spatial separation of the links can be obtained in the elevation domain as well as the azimuth domain. This leads to an increase in throughput and system robustness; further advantages of FD-MIMO systems include simplified signal processing and the reduction in energy consumption since the transmit energy can be focused very precisely towards the intended receiver.

An essential step in the design of an FD-MIMO wireless system is the measurement and modeling of the propagation channel in which this system is to operate. Hence, comprehensive and realistic characterization of multidimensional properties of the multipath components (MPCs), in particular azimuth and elevation, is essential.

Massive MIMO systems will be deployed first in urban macrocells, since those require the highest capacity. The current paper thus concentrates on this environment.

A. Related works

Several publications [10]–[19] have investigated the 3D characterization of urban macrocellular propagation channels. Some of these publications considered elevation parameters at *one* link-end only, i.e., either Multiple-Input-Single-Output (MISO) [10], [13], [12] or Single-Input-Multiple-Output (SIMO) [14], [16] setups. [15] conducted 3D MIMO measurements using a planar array at 2.6 GHz and bandwidth of 65 MHz, however, the results presented were constrained to an angular spread analysis at the Base Station (BS). Other publications [17], [18], [19] explored 3D Outdoor-to-Indoor (O2I) urban macro/microcellular environments, however, these were done using ray-tracing simulations. Measurements were performed in an environment and with a measurement setup similar to ours in [11], however this was done using a different antenna array structure and not all parameters needed to fully characterize and develop a double-directional polarimetric propagation channel model were provided. A 3D channel model was developed in [20] using a geometry based stochastic model (GSCM) (following the cluster-based approach common to COST 259, 273 and 2100 as well as SCM, WINNER II models); however, the actual statistical values for channel parameters needed for a double-directional model were not provided in the paper. Ref. [21] conducted 3D measurements in an urban macrocell (with very large and regular high-rise buildings) environment, however, this environment differs

Part of this work was presented at MILCOM 2015 [1].

S. Sangodoyin, V. Kristem, C.U. Bas and A.F. Molisch are with the Department of Electrical Engineering, University of Southern California (USC), Los Angeles, CA 90089-2560 USA. J. Lee is with Samsung, Korea. J. Zhang is with Samsung USA, Dallas, TX, USA. M. Käske, C. Schneider, G. Sommerkorn and R. Thomä are with institut für informationstechnik, Technische Universität Ilmenau, Ilmenau, Germany.

[1]Most panel arrays, such as rectangular and cylindrical, are in fact 2D arrays, yet they are commonly called 3D to indicate that the signal properties at their antenna elements are impacted by both elevation and azimuth of the multipath components.

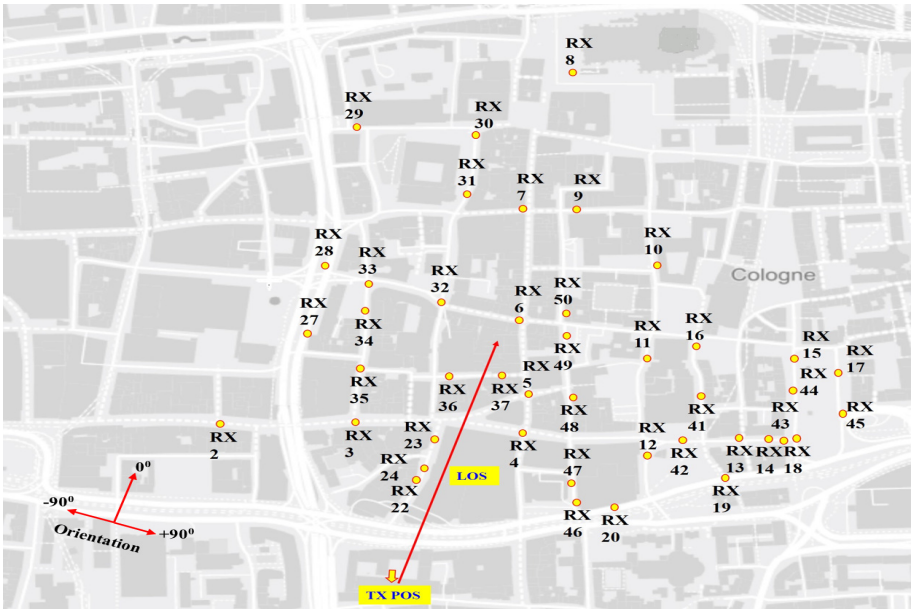

Fig. 1: Map of measurement area in Cologne.

from ours which comprised of an irregularly built-up, Europe-style old city. Also, the measurements were conducted on a dense grid in a wide street while our measurements were conducted at isolated points, which are much more separated. Finally, the sounder setup in [21] precluded 360 degree visibility of paths at the mobile station, as is used in our paper. In our conference paper [1], we provided preliminary results for the channel measurement campaign that underlies the current paper, in particular, path distribution and MPC cluster parameters, however, we did not provide other channel parameters (and their statistics) needed for modeling a 3D full-polarimetric urban macrocellular channel. For an overview of other related literature, we refer the interested reader to our recent review [22] and [23].

B. Contribution

As seen from the literature review above, there is a dearth of investigations of 3D MIMO propagation channel measurements and modeling in urban environments. The current paper aims to partly fill this gap. The contributions of this paper can be summarized as follows:

- We provide a detailed description of the measurement setup and procedure using an advanced polarimetric wideband FD-MIMO channel sounder with massive number of antenna elements.
- We extract MPCs through a high-resolution algorithm, group them into clusters and derive both *intra-* and *inter-*cluster statistics.
- We provide a parameterization of the model for the Dense Multipath Components (DMC) in the measured environment. Such an analysis of DMC in a 3D urban macrocellular environment has not been done before.
- We develop a double directional cluster-based channel model, which is validated by comparing the resulting delay spread and direction spread to those obtained from the raw data.

C. Organization

This paper is organized as follows. Section II describes the measurement environment and the measurement setup. Section III describes the signal modeling procedure. Results for the extracted MPCs are presented in Section IV. Section V describes the model validation procedure. Summary and conclusions are provided in Section VI.

II. Measurement Campaign

A. Measurement environment

We carried out the measurement campaign in Cologne (Germany). The structural layout of the city has been discussed in [1], while Fig. 1 shows the map of the area covered during our measurement campaign with the different receiver (RX) locations indicated as well as BS position and its orientation. The transmitter (TX) was mounted on the rooftop of a 30 m high-rise building just outside the old city center, see Fig. 2. The RX was placed on the rooftop of a car at about 2.5 m height above ground. The measurements were conducted at multiple RX positions in street canyons, alleys and open squares. The measurements were done in the frequency band from 2.52-2.54 GHz, which the owner of the band, Deutsche Telekom, made available for our measurements. This also guaranteed absence of interference, and precisely limited the bandwidth we could use for the measurements.

B. Measurement setup

A key component of our measurement setup is the MEDAV RUSK sounder [24], [25] – a wideband polarimetric MIMO channel sounder. This sounder is based on the switched array principle: the transmit signal, which is a multi-carrier signal,

Fig. 2: TX view of the urban macrocell in Cologne.

is up-converted (via a *single* RF chain) to passband and then is connected, via a fast electronic switch, to the antenna elements of the transmit array one by one. Similarly, on the receive side, the signals from the antenna elements are connected to the receive chain sequentially [26]. This type of measurement provides a full channel characterization as long as all TX/RX antenna combinations are measured within a time that is shorter than the coherence time of the channel. Sounders based on this principle have been used extensively, e.g., [26], [24]. An illustration of the sounder setup is shown in Fig. 3, while a system diagram is provided in Fig. 5.

A cylindrical antenna array structure was used at both TX and RX. The TX array was constructed from a synthetic aperture setup such that a switched 8-element (2 port per element) polarimetric uniform linear patch array (PULPA, shown in Fig. 4(a)) was mechanically rotated into different directions. To increase the gain of the PULPA in azimuth, a stack of 4 horizontally placed antenna elements were connected by a pre-configured, controlled, power divider (equal-split) array feeder network to form a narrow transmit beam in azimuth (i.e., restricting azimuth opening angle). The PULPA was placed on a programmable positioner that was rotated in an azimuth angular range from -180^o to 180^o with a 6 degree step-size to create 60 virtual positions, thereby imitating a cylindrical array structure. This resulted in a virtual (16 x 60) TX antenna array (all ports considered). This TX structure is referred to as vertical stacked polarimetric uniform circular patch array (VSPUCPA). The antenna elements used in this setup have a 3 dB beamwidth of 100 degrees in elevation and 26 degrees in azimuth. Additional details on the TX array are provided in [1].

At the receiver, a purely switched approach (without positioner) was used: a stacked polarimetric uniform circular patch array (SPUCPA, shown in Fig. 4(b)) with 2 (vertical) x 8 (circumference) x 2 (polarization) antenna ports was employed. The impact of the sounder characteristics and the antenna arrays are measured and stored for post-processing (see Sec. IV) during back-to-back calibration, and antenna calibration in an anechoic chamber, respectively.

Rubidium (Rb) clocks are used at both TX and RX end for timing and frequency control of the sounder. Also, the trigger signal between the TX and RX ends was sent over-the-air using a cellular (Universal Mobile Telecommunications Service (UMTS)) connection.

Clock drifts of the local oscillators were observed in preliminary anechoic chamber measurements. The clock drift can have a significant impact on the measurements results. Details of the phase-drift correction techniques are given in [1], [27].

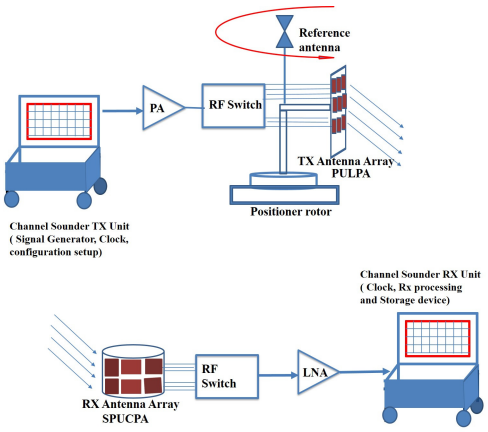

Fig. 3: Illustration of channel measurement sounder.

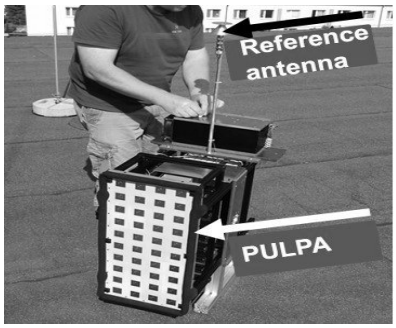

(a) PULPA and reference antenna

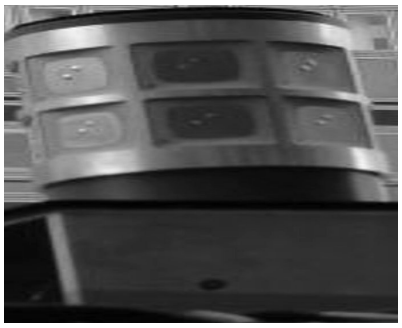

(b) RX-SPUCPA

Fig. 4: TX antenna array (PULPA) and RX antenna array (SPUCPA)

TABLE I: Channel sounder configuration.

Parameters	**Values**
Bandwidth	2.52 GHz-2.54 GHz
No. of frequency points, M_f	257
Number of channels	900 x 32
Total time syn. aperture	approx. 10mins
Tx ports, Rx ports	900 ports, 32 ports
Polarization	H/V
Azimuth range	$[-180^\circ$ to $180^\circ]$
Elevation range	$[90^\circ$ to $-90^\circ]$

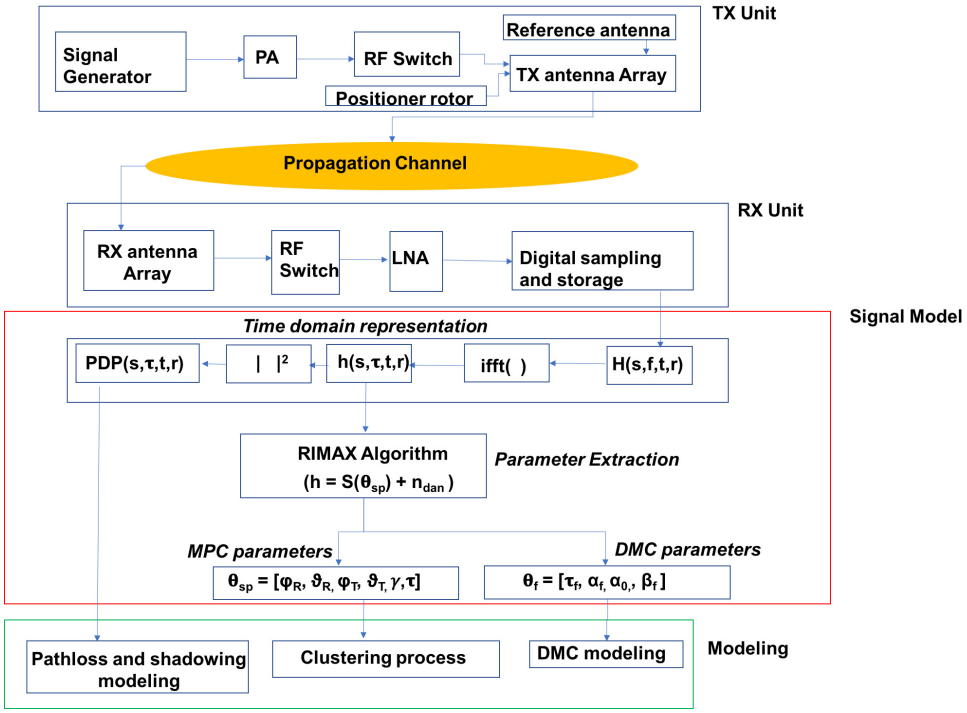

Fig. 5: System diagram of the channel sounder setup and data processing.

III. Signal Model

This section presents the transfer function data structure, time domain representation and parameter extraction procedure that form the basis of the post-processing of the data.

A. Time-domain representation

The transfer function of the measured propagation channel is a order-4 tensor $H(s, f, t, r)$ from which the spatio-temporal information of the MIMO radio channel can be derived. Here s denotes the measured snapshot index, f is the measured frequency index with $f = 1, ..., M_f$, where M_f is the number of measured frequency points. t and r represent the TX and RX antenna elements index respectively with $t = 1, ..., M_T$ and $r = 1, ..., M_R$. M_T, M_R are the number of TX and RX elements. To improve the signal-to-noise ratio (SNR) of the measurement, 10 snapshots were recorded for each TX/RX antenna pair and averaged during post-processing. The channel impulse response $h(s, \tau, t, r)$, where τ indicates delay, is obtained from the transfer function by inverse Fourier transform with Hanning window to suppress aliasing. The local power-delay profile (PDP) is computed as $PDP(s, \tau, t, r) = |h(s, \tau, t, r)|^2$.

B. Parameter extraction

To obtain a channel characterization that is independent of the antenna structure, one normally obtains a double-directional channel characterization that extracts the spatio-temporal-polarimetric parameters of the MPCs from the transfer function through the use of a high resolution parameter estimation (HRPE) algorithm. The HRPE algorithm that was used in the work is RIMAX – an iterative maximum-likelihood estimator. An extensive description of the parameter extraction procedure of RIMAX is provided in [28]. It differs from other popular algorithms by modeling the propagation channel ($\mathbf{h}$) as a superposition of specular/deterministic paths ($\mathbf{S}(\theta_{\text{sp}})$), dense multipath components (DMC, $\mathbf{D}(\theta_{\text{dmc}})$) and measurement noise ($\mathbf{n}$):

$$\mathbf{h} = \mathbf{S}(\theta_{\text{sp}}) + \mathbf{D}(\theta_{\text{dmc}}) + \mathbf{n} \quad \in \quad \mathbb{C}^{M_T M_R M_f \times 1}, \tag{1}$$

The DMC, which describes the stochastic part of the propagation channel, is assumed to comprise of a large number of individually weak signal components that cannot be estimated individually as plane waves, e.g., because of the underlying physical process (diffuse scattering, wavefront curvature, etc.). Therefore, owing to the central limit theorem, $\mathbf{D}$ (to simplify our notation, we will denote $\mathbf{D}(\theta_{\text{dmc}})$ as $\mathbf{D}$ henceforth) is modeled as a zero-mean complex circularly symmetric Gaussian distributed random vector with a covariance matrix $\mathbf{R}_{\text{D}} \in \mathbb{C}^{M_T M_R M_f \times M_T M_R M_f}$, i.e., $\mathbf{D} \sim \mathcal{N}_c(0, \mathbf{R}_{\text{D}})$. The measurement noise[2] is assumed to be a white complex circularly symmetric Gaussian distributed random vector $\mathbf{n} \sim \mathcal{N}_c(\mathbf{0}, \sigma_{\text{N}}^2 \mathbf{I})$ with variance σ_{N}^2 .

For simplicity, DMC and noise were modeled together to form a zero-mean complex Gaussian process with covariance matrix:

$$\mathbf{R}_{\text{dan}} = \mathbf{R}_{\text{D}} + \sigma_{\text{n}}^2 \mathbf{I}. \tag{2}$$

This implies that (1) can be written in a more compact form:

$$\mathbf{h} = \mathbf{S}(\theta_{\text{sp}}) + \mathbf{n}_{\text{dan}} \quad \in \quad \mathbb{C}^{M_T M_R M_f \times 1}, \tag{3}$$

[2]The measurement noise results from both thermal noise from the electronics as well as ambient noise.

where $\mathbf{n}_{\text{dan}} \sim \mathcal{N}_c(0, \mathbf{R}_{\text{dan}})$.

In the estimator, specular components ($\mathbf{S}(\theta_{\text{sp}})$), or plane waves, are characterized by the time-delay (τ), angle-of-arrival (azimuth (φ_{R}) and elevation (ϑ_{R})), angle-of-departure (azimuth (φ_{T}) and elevation (ϑ_{T})) and the complex polarimetric path-weights (γ), i.e., $\theta_{\text{sp}} = [\varphi_{\text{R}}, \vartheta_{\text{R}}, \varphi_{\text{T}}, \vartheta_{\text{T}}, \gamma, \tau]$ such that

$$\mathbf{S}(\theta_{\text{sp}}) = \sum_{l=1}^{L} \mathbf{B}_{\text{R}}^{T}(\varphi_{\text{R},l}, \vartheta_{\text{R},l}) \cdot \begin{bmatrix} \alpha_{\text{HH},l} & \alpha_{\text{HV},l} \\ \alpha_{\text{VH},l} & \alpha_{\text{VV},l} \end{bmatrix} \cdot \mathbf{B}_{\text{T}}(\varphi_{\text{T},l}, \vartheta_{\text{T},l}) \cdot e^{-j2\pi f \cdot \tau_l}, \quad (4)$$

where the superscript T denotes the transpose operator, $\mathbf{B}_{\text{R}}$ and $\mathbf{B}_{\text{T}}$ are the nonlinear mappings of the angles of arrival ($\varphi_{\text{R}}, \vartheta_{\text{R}}$) and departure ($\varphi_{\text{T}}, \vartheta_{\text{T}}$) to the antenna array responses and are obtained from calibration measurements in an anechoic chamber. The parameters $\alpha_{\text{HH},l}, \alpha_{\text{HV},l}, \alpha_{\text{VH},l}, \alpha_{\text{VV},l}$ and τ_l denote the radio wave polarization amplitudes (horizontal-to-horizontal (HH), horizontal-to-vertical (HV), vertical-to-horizontal (VH), vertical-to-vertical (VV)) and the time-delay of the l-th path respectively.

IV. Results

We next discuss the path distribution in the environment, followed by a clustering analysis, and the *intra-* and *inter-*cluster statistics. Large scale parameters such as pathloss and shadowing as well as the dense multipath components are also discussed in subsequent subsections.

A. Path distribution in the environment

To provide insights into the propagation mechanisms in the environment, we first show results from a sample NLOS location (position 47 indicated in Fig. 6). Fig. 6 shows propagation paths and interacting objects (IOs) encountered along the paths by the MPCs; in this and the subsequent plots not all extracted MPCs are shown to avoid congestion of the figures. The arrows P1, P2 and P3 shown in Fig. 6 are in fact not representing a single MPC but groups of MPCs propagating along these routes. A spherical coordinate system has been used with orientation expressed such that the azimuth angle is defined clockwise from $-180°$ to $0°$ to $180°$ (with $0°$ indicating the PULPA orientation towards the LOS as shown in Fig. 1), while the elevation angle is defined from $90°$ to $0°$ to $-90°$, where $90°$ indicates the north pole, $0°$ indicates the equatorial plane and $-90°$ indicates the south pole. Looking at the direction-of-departure (DoD) azimuth - delay, DoD elevation - delay plots shown in Figs. 7(a) and 7(b), it can be observed that MPCs having $\varphi \approx 30°$, $\vartheta \approx -6°$, and $\tau \approx 245\,\text{m}/\text{c}_0$[3] propagate via rooftop diffraction (Quasi-LOS, P2 on Fig. 7(a) and 7(b)), while MPCs occurring in the range $\varphi \approx 20° - 26°$ and $\vartheta \approx -6°$ were initially reflected off the Galeria Kaufhof (P1, see Fig. 6, 7(a) and 7(b)) and then propagated through the street canyon (SC 1 on Fig. 6) acting as a waveguide. MPCs with azimuth angles between $39° - 40°$ and elevation of about $-5°$ (P3, Fig. 6, 7(a) and 7(b)) are deemed to have been reflected off the Inter-Continental building initially and then propagate through the street canyon (SC 2, also in Fig. 6). Other observable MPCs with large delay (about 600 m) and elevation angle of about $-1.5°$ to $-3°$ are contributions from far-away scatterers.

A similar analysis was implemented on all other measurement points, and we determined probable routes and IOs as well. This serves not only to gain insights into the propagation mechanisms of MPCs in the urban macrocellular environment, but also to validate the high-resolution parameter extraction procedure. Similar analyses were also performed in [12], [13] and [29]. A detailed discussion of the propagation mechanisms of MPCs in this environment is provided in [30].

As a further check for the validity of our high-resolution parameter extraction procedure, we evaluated the relative residual power error (Δ_{p}) between the power of the measured transfer function and that of the reconstructed transfer function (obtained using RIMAX results). The relative residual power error was calculated as: $\Delta_{\text{p}} = \frac{|\text{P}-\hat{\text{P}}|}{|\text{P}|}$, where P denotes the power of measured channel and $\hat{\text{P}}$ denotes the power[4] of the reconstructed channel (with DMC power included). Δ_{p} obtained in our analysis was 2.3%. Note that this is the power not contained in *either* the discrete MPCs or the DMC, and thus different from the difference between total power and specular MPC power that was used in other papers to assess the importance of non-discrete MPCs.

Another observations is that the aforementioned MPCs naturally grouped into clusters. This clustering phenomenon of MPCs is discussed subsequently.

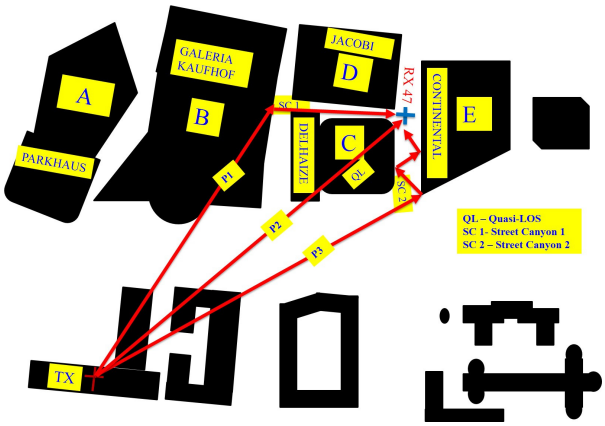

Fig. 6: Illustration of receiver position 47.

B. Clustering analysis

We define a cluster as a group of MPCs whose parameter values in all dimensions, i.e., delay, azimuth and elevation at TX and RX are very similar, while being notably different from those of other MPCs in at least one dimension. Clustering allows a more compact channel description through the use of intra- and inter-cluster distributions, and thus has been adopted in modern channel models such as COST 259 [31], [32], 3GPP SCM [9], ITU-Winner [33], and COST 2100 [34].

[3]Note that $\text{c}_0 \approx 3$ x 10^8m/s denotes the speed of light in vacuum.

[4]Note that the power was averaged over all polarization.

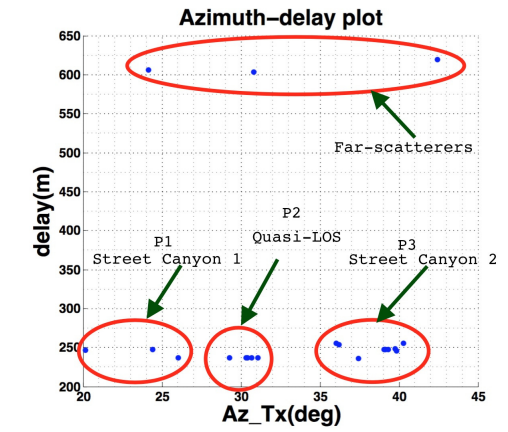

(a)

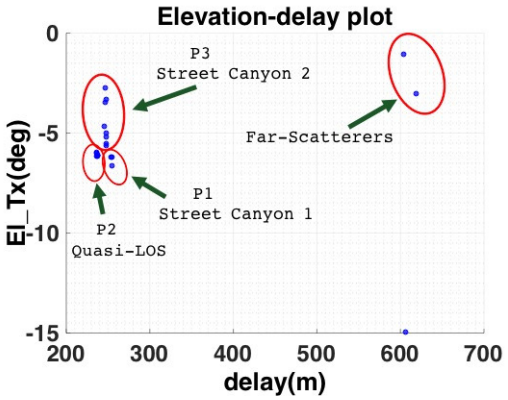

(b)

Fig. 7: (a) DoD (az-delay) plot of extracted MPCs. (b) DoD (el-delay) plot of extracted MPCs.

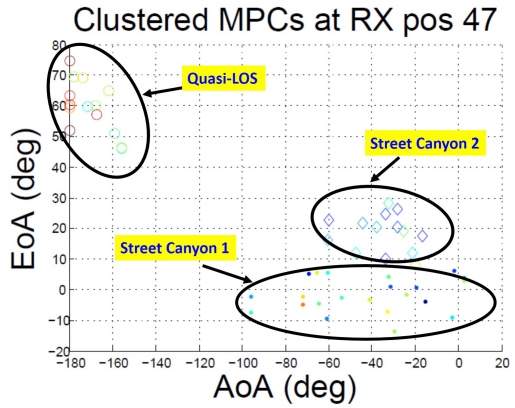

Fig. 8: Clusters at RX position 47.

In our work, we use the K-power means clustering algorithm [35], [36], [37], [38], [39], along with visual inspection (as done in [40], [41], [42]) to obtain a reasonable number of clusters. We then proceed to estimate cluster angular and delay statistics. Note that the cluster angular parameters include elevation-of-departure (EoD), elevation-of-arrival (EoA), azimuth-of-departure (AoD) and azimuth-of-arrival (AoA).

Sample clustering results for RX position 47 are shown in Fig. 8. From this plot, it is clearly observable that these clusters stem from the different IOs (shown in Fig. 6). Similar clustering analyses were performed for all other measured locations. Statistics of the aforementioned parameters inherent to the clusters can be used in our modeling process.

C. Clustering statistics

A statistical channel model is developed based on the results from the clustering analysis. From [31], the generic form of the impulse response $h^{'}$ of the channel can be represented as:

$$h^{'}(\tau, \Omega_{\text{TX}}, \Omega_{\text{RX}}) = \sum_{m=1}^{M} \sum_{n \in C_m} h_n^{'}(\tau, \Omega_{\text{TX}}, \Omega_{\text{RX}}), \quad (5)$$

where indices of the MPCs $h_l(\tau, \Omega_{\text{TX}}, \Omega_{\text{RX}})$, $l = 1, ..., L$ can be grouped into $M \leq L$ *disjoint* clusters

$$C_1, ..., C_M, \quad (6)$$

with each cluster having $N_m \geq 1$ elements, and

$$\sum_{m=1}^{M} N_m = L. \quad (7)$$

Cluster-based channel models are characterized by two sets of parameters, namely *intra-* and *inter*-cluster parameters. The *inter*-cluster parameters are cluster time-of-arrival (ToA, T_m), cluster DoD (Ω_{TX_m}), cluster direction-of-arrival (DoA) (Ω_{RX_m}), cluster power, and number of clusters (M). The *intra*-cluster parameters include MPC ToA ($\tau_{m,n}$), MPC DoA ($\zeta_{m,n}$), MPC DoD ($\psi_{m,n}$), MPC complex amplitude ($\beta_{m,n}$) and the number of MPCs (n) per clusters. For ease of discussion and similarity to what is available in the literature, we will henceforth refer to MPCs as rays.

Following the Saleh-Valenzuela model [43], the cluster and ray arrival time distributions may be described by two Poisson processes, which implies that the cluster inter-arrival times and ray intra-arrival times are typically described by two independent exponential probability density functions (PDFs) as follows:

$$p(T_m|T_{m-1}) = \Lambda \cdot e^{-\Lambda(T_m - T_{m-1})}, \quad m > 0, \quad (8)$$

$$p(\tau_{m,n}|\tau_{m,n-1}) = \lambda \cdot e^{-\lambda(\tau_{m,n} - \tau_{m,n-1})}, \quad n > 0, \quad (9)$$

where Λ is the mean cluster arrival rate and λ is the mean ray arrival rate.

1) Intra-cluster parameters: The *intra*-cluster parameter ToA of rays within each cluster is defined relative to the smallest arrival time of all the rays within the cluster.

The cluster and ray power was modeled as

$$\overline{\beta_{m,n}^2} = \overline{\beta(0,0)^2} \cdot e^{-\frac{T_m}{\Gamma}} \cdot e^{-\frac{\tau_{m,n}}{\gamma}} \cdot P_{\Omega_{\text{TX}_m}} \cdot P_{\Omega_{\text{RX}_m}}, \quad (10)$$

where Γ and γ are the cluster and ray decay constants, respectively, and $\overline{\beta(0,0)^2}$ is the average power of the first ray in the first cluster [44]. $P_{\Omega_{\text{TX}}}$ and $P_{\Omega_{\text{RX}}}$ are intra-cluster distribution in the angular domain (power angular spectra) and are modeled, both in the azimuth and elevation domains, using the Laplacian distribution which is of the form:

$$P_\Omega(\Omega) = \frac{1}{2\sigma_\Omega} \cdot e^{-\frac{|\Omega-\Omega_n|}{\sigma_\Omega}}. \quad (11)$$

DoA/DoD are defined relative to the cluster center, which is computed as the power-weighted mean of DoA/DoD of all rays within the cluster. The measured distributions of the intra-cluster angular parameters at a sample location as well as their comparison to the Laplacian fit is shown in Figs. 9(a) - 9(d). The distribution (using an ensemble of all measured locations) of the spread of these angular parameters are modeled by lognormal distribution. The parameters of the lognormal distribution are shown in Table IV. Parameters λ, Λ, Γ and γ have been extracted as done in [44] and [45] with values also provided in Table IV.

The delay between the ToAs of sucessive rays is modeled using an exponential distribution as described in (9). The PDP of each cluster is a one-sided exponentially decaying function as can be seen from (10). All cluster spreads (angular and delay) were found to be lognormally distributed with the mean and variance provided in Table IV. Correlation between cluster parameters[5] was explored in our work with correlation coefficient values provided in Table IV. The ray arrival rate λ, and the inter-cluster parameters Γ and Λ are modeled as constants. The number of rays per cluster were modeled with an exponential distribution, where the average number of rays per cluster was approximately 16.

2) Inter-cluster parameters: In the *inter*-cluster case, we define the angular and delay parameters for each cluster center relative to the geometric LOS connection (which is defined irrespective of whether a LOS MPC exists or not). The ToA of this LOS connection is given by the Euclidean distance between the TX and RX array at each measurement location, while the DoA and DoD are determined by the orientation/alignment of the RX relative to LOS during the channel measurement.

We found the relative cluster EoD and EoA to be Laplacian distributed, while the relative AoD follows a Gaussian distribution. Also, the relative AoA was found to follow a uniform distribution in the range $[-\pi, \pi)$. Figs. 10(a)-10(d) show the aforementioned distribution fits while the parameters of these distributions are provided in Table IV. Note that the selected distribution fits had the highest passing rates (at 5% signifcance level) when compared to other candidate distributions in a Kolmogorov-Smirnov (K-S) hypothesis test [46]. The K-S procedure is a standard nonparametric hypothesis test of the equality of continuous, one dimensional probability distributions. It is based on the maximum difference between an empirical and a hypothetical cumulative distribution. The *inter*-cluster parameters were found to be uncorrelated, which is understandable due to the NLOS nature of the environment and the cluster-based modeling procedure. However, cluster parameters might in fact be correlated when using a class-based modeling (i.e., grouping clusters into classes) as in [30].

The cumulative distribution function (CDF) of the number of clusters from all measured locations in the urban environment is shown in Fig. 11. Although some works have reported smaller values in urban environments [32], others such as [12] show quite similar results. The number of clusters N_k can be modeled (similarly to the COST 259 model) as $N_k = N_{c_{min}} + X$, where $N_{c_{min}} = 1$ is the minimum number of clusters, while X is a Poisson distributed random variable with an average rate (η_c) of 2.18.

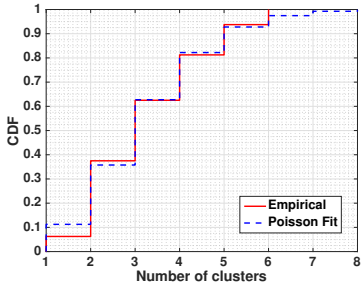

Fig. 11: Distribution of the number of clusters.

The cluster shadowing gain (SF) is defined as the deviation of the cluster power from its expected value [47], which in turn can be derived from the estimation of the cluster power decay constant (Γ, see (10)). In other words, when the cluster power decay constant is estimated, the linear regression fit provides an expected cluster power for a certain relative cluster delay. The cluster shadowing in our analysis is modeled to be lognormally distributed, i.e., its logarithmic value is approximated by a zero-mean Gaussian distribution (as shown in Fig. 12) with standard deviation (σ_{cl}) of 7.47 dB. We can see that the fit is somewhat loose; however, since lognormal distribution of shadowing gains is widely used in the literature, we adhere to this convention.

The lognormal distribution was confirmed by matching the empirical data to some typical theoretical distribution such as lognormal, Nakagami, Rayleigh, Ricean, and Weibull. The K-S hypothesis test was used to determine the goodness-of-fit (GOF) of these distribution at 5% significance level. Results of the K-S test are shown in Table II below, it can be seen that the lognormal distribution gives the highest passing rate.

D. Cluster polarization

A complete channel model requires the description of the

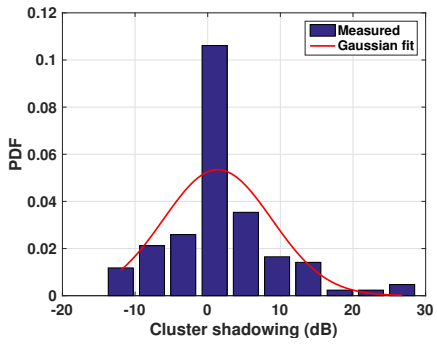

Fig. 12: PDF of cluster shadowing gain.

[5]We used the logarithmic values of the parameters.

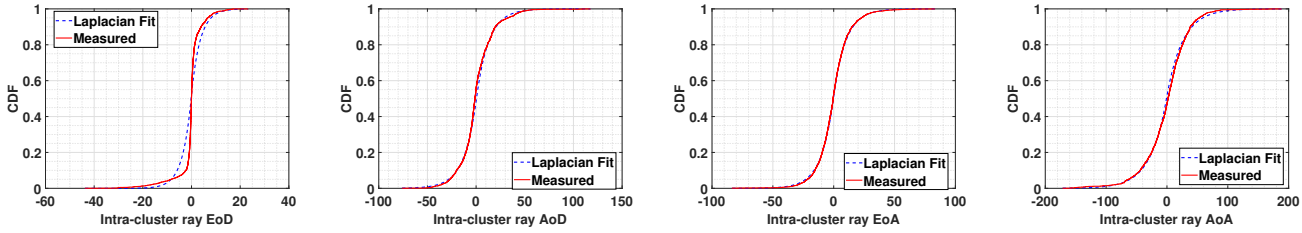

(a) EoD. (b) AoD. (c) EoA. (d) AoA.

Fig. 9: Distribution of the *intra*-cluster angular (centered) parameters of rays for a sample location.

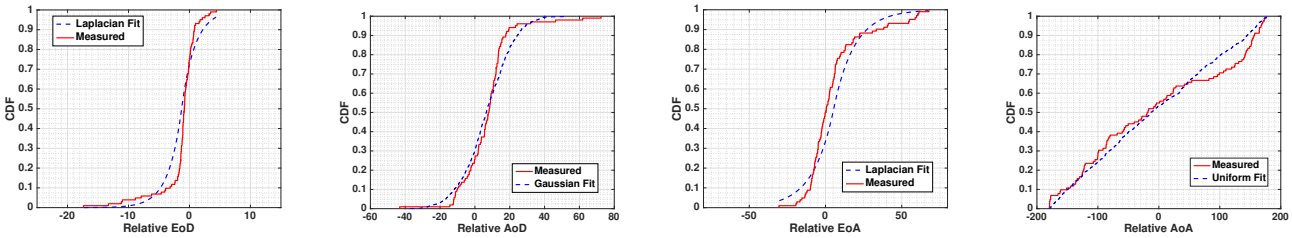

(a) EoD. (b) AoD. (c) EoA. (d) AoA.

Fig. 10: Distribution of the *inter*-cluster angular parameters.

TABLE II: Passing rate of K-S test at 5% significance level.

Distribution	K-S
Weibull	81.57
Rayleigh	65.87
Rician	65.87
Lognormal	92.36
Nakagami	66.36

polarization [48], [49] and [50]. The cluster polarization can be described by a two-by-two polarimetric matrix $\mathrm{A_{pol}}$,

$$\mathrm{A_{pol}\,[dB]} = \begin{bmatrix} \mathrm{CPR_{HH}} & \mathrm{XPR_{HV}} \\ \mathrm{XPR_{VH}} & \mathrm{CPR_{VV}} \end{bmatrix}, \tag{12}$$

where the co- and cross-polarization ratios are represented as CPR and XPR while V and H denote vertical and horizontal polarization respectively. The off-diagonal element, $\mathrm{XPR_{HV}}$ (see (13)) describes the (total power) crosstalk from horizontal to vertical polarization of MPCs within a cluster (and similarly for $\mathrm{XPR_{VH}}$ (see (14))).

$$\mathrm{XPR}^{m}_{\mathrm{HV}}(\mathrm{dB}) = 10 \cdot \log_{10}\left(\frac{\sum_{n=1}^{N_m} |\alpha_{\mathrm{HH},m,n}|^2}{\sum_{n=1}^{N_m} |\alpha_{\mathrm{HV},m,n}|^2}\right) \tag{13}$$

$$\mathrm{XPR}^{m}_{\mathrm{VH}}(\mathrm{dB}) = 10 \cdot \log_{10}\left(\frac{\sum_{n=1}^{N_m} |\alpha_{\mathrm{VV},m,n}|^2}{\sum_{n=1}^{N_m} |\alpha_{\mathrm{VH},m,n}|^2}\right) \tag{14}$$

On-diagonal elements $\mathrm{CPR_{HH}}$ and $\mathrm{CPR_{VV}}$ represent the ratio of the co-polarized component compared to the total power. From our analysis, XPR in dB is approximately Gaussian distributed with a 6 dB average and a standard deviation of 1.5 dB. The occurrence of this distribution for XPR had

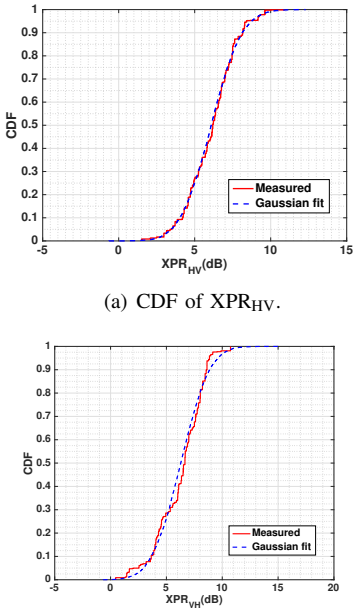

(a) CDF of $\mathrm{XPR_{HV}}$.

(b) CDF of $\mathrm{XPR_{VH}}$.

Fig. 13: Distribution of the XPR.

been reported in the literature [32], [51] and [52] for different environments and is confirmed by Figs. 13(a) and 13(b). Parametric values for this distribution are provided in Table IV below. Note that depending on the propagation conditions, $\mathrm{XPR_{HV}}$ can be different from $\mathrm{XPR_{VH}}$. Also, within each cluster, the XPR of rays ($\bar{\mathrm{XPR}}$) can also be modeled as a Gaussian distributed variable with mean value as the cluster XPR while the standard deviation values are 4.19 for $\bar{\mathrm{XPR}}_{\mathrm{HV}}$ and 4.52 for $\bar{\mathrm{XPR}}_{\mathrm{VH}}$.

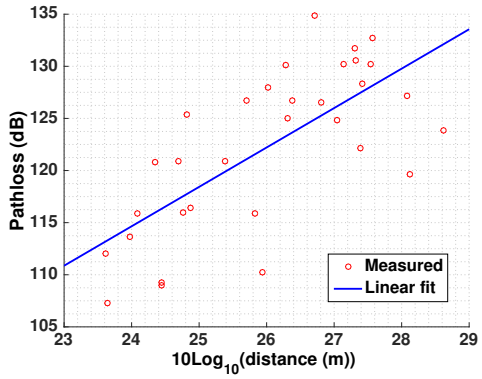

Fig. 14: Linear regression fit for pathloss and delay.

E. Pathloss and shadowing model

Pathloss model: Following the literature, we use a conventional power law equation [53], [54] to model the distance-dependent pathloss P_{L} in dB (also known as $\alpha - \beta$ model [55]):

$$P_{\mathrm{L}}(d) = P_0 + 10 \cdot \xi \cdot \log_{10}\left(\frac{d}{d_0}\right) + \chi_\sigma, \tag{15}$$

where d_0 is the reference distance namely 1 m, P_0 is the (fitted) pathloss at the reference distance, ξ is the pathloss exponent and χ_σ is a random variable describing large-scale variations (in dB) due to shadowing; adhering to the literature [56] and [57], we model the shadowing by a lognormal (i.e., Gaussian on a dB scale) distribution. Fig. 14 shows the scatter plot of P_{L} for all measurements conducted at different distances and a linear regression fit. All parameters extracted are provided in Table IV. Of course, the fit is only valid for the distance range of 200-728 m, namely the distances for which underlying measurements exist.

Shadowing: The bulk[6] shadowing gain (denoted as χ_σ in (15)) accounts for the large-scale fluctuation of the received power. We see that, in agreement with the modeling assumption in (15), the logarithmic value of the measured deviation closely matches a zero-mean Gaussian distribution ($N(0, \sigma_\chi[dB])$) (see Fig. 15 and Table IV).

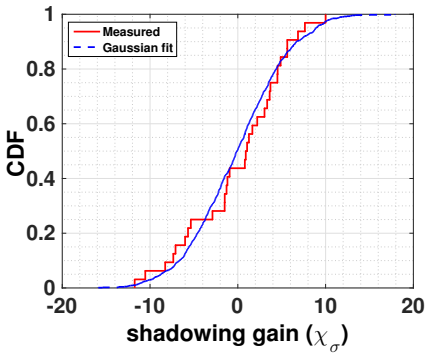

Fig. 15: CDF of the bulk shadowing gain.

[6]The term *bulk* denotes that we are analyzing the shadowing using the entire channel response.

The lognormal distribution was confirmed here as well by using a K-S hypothesis test to determine the GOF of different candidate distributions at 5% significance level, see Table III.

TABLE III: Passing rate of K-S test at 5% significance level.

Distribution	K-S
Weibull	69.48
Rayleigh	15.39
Rician	15.38
Lognormal	95.41
Nakagami	22.68

F. Dense multipath component (DMC)

The DMC consists mainly of a large amount of weak MPCs originating from, e.g., scattering from objects that are either small in size compared to the wavelength or have rough surfaces [58], [59]. It is usually described as the residual after the specular component in the channel response has been extracted.

Although more sophisticated techniques have been introduced in [60] and [61] to advance the modeling of DMC, in our work we adhere to the DMC model as discussed in [28], [62], [63]. The analysis in this work is done over an aggregate of the different polarization components.

The DMC is described by its covariance matrix $\mathbf{R}_{\mathrm{D}}$ (see (2)) and can be decomposed into the Kronecker-product of three matrices:

$$\mathbf{R}_{\mathrm{D}} = \mathbf{R}_{\mathrm{R}} \otimes \mathbf{R}_{\mathrm{T}} \otimes \mathbf{R}_{\mathrm{F}}, \tag{16}$$

where $\mathbf{R}_{\mathrm{F}}$ is the covariance matrix in the frequency domain while $\mathbf{R}_{\mathrm{R}}$ and $\mathbf{R}_{\mathrm{T}}$ are the covariance matrices of the antenna array elements at the TX and RX.

The frequency domain covariance matrices can be modeled by:

$$\mathbf{R}_{\mathrm{F}} = \mathrm{toep}(\bar{\lambda}(\theta_{\mathrm{F}}), \bar{\lambda}(\theta_{\mathrm{F}})^\dagger), \tag{17}$$

where the operator $\mathrm{toep}(\cdot)$ denotes a Toeplitz matrix [64], [65] and $\bar{\lambda}$ is a sampled version of the power spectral density, given by

$$\bar{\lambda}(\theta_{\mathrm{F}}) = \frac{\tilde{\alpha}_1}{M_f}\left[\frac{1}{\tilde{\beta}_{\mathrm{d}}}, \frac{e^{-j2\pi\tau_{\mathrm{d}}}}{\tilde{\beta}_{\mathrm{d}} + j2\pi\frac{1}{M_f}}, \cdots, \frac{e^{-j2\pi(M_f-1)\tau_{\mathrm{d}}}}{\tilde{\beta}_{\mathrm{d}} + j2\pi\frac{M_f-1}{M_f}}\right]^T. \tag{18}$$

The parameters of the frequency domain covariance matrix model are

$$\theta_{\mathrm{F}} = [\tau_{\mathrm{d}},\ \tilde{\beta}_{\mathrm{d}},\ \tilde{\alpha}_1]^T, \tag{19}$$

where β_{d} is the normalized[7] coherence bandwidth of the channel, τ_{d} and $\tilde{\alpha}_1$ are the delay of arrival and power of the first component in the time domain[8] equivalent of (17).

The spatial covariance matrices ($\mathbf{R}_{\mathrm{T}}$ and $\mathbf{R}_{\mathrm{R}}$) can be modeled as:

$$\mathbf{R}_{\mathrm{R/T}} = \mathbf{B}_{\mathrm{R/T}} \cdot \mathbf{K}(\theta_{\mathrm{R/T}}) \cdot \mathbf{B}_{\mathrm{R/T}}^\dagger, \tag{20}$$

[7]Note that the normalization is done with the measurement bandwidth.
[8]This is obtained by using an inverse Fourier transform.

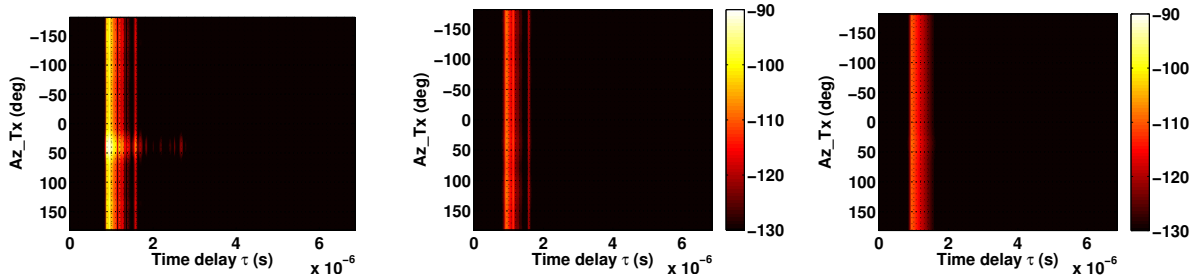

(a) Measured total. (b) Residual. (c) Modeled residual.

Fig. 16: Comparison of (a) measured (**h**) (b) residual ($\mathbf{h} - (\mathbf{S}(\theta_{\text{sp}}))$) and (c) modeled DMC Power-azimuth-delay-profile (PADP) at Tx end for Rx Position 47.

where $\mathbf{B}_{\text{R/T}}$ denotes the antenna array responses at RX and TX, while $\mathbf{K}(\theta_{\text{R/T}})$ is a diagonal matrix whose entries are determined by the angular probability density distribution of the DMC, which is modeled as a Von-Mises distribution (VMD) [62]. Superscript † denotes Hermitian transpose. The PDF for the one-dimensional case is defined as:

$$f_{\varphi}(\varphi, \mu, \kappa) = \frac{1}{2\pi \cdot I_0(\kappa)} \cdot e^{\kappa \cdot cos(\varphi - \mu)} \tag{21}$$

where μ is the mean angle, κ the concentration parameter, and I_0 the modified Bessel function of the first kind of the order zero. A beamformer approach is discussed in [62] where an additional uniform distribution (UD) with magnitude $\bar{\alpha}$ is introduced such that (21) is modified to:

$$f_{\varphi,\text{UD}}(\varphi, \mu, \kappa, \bar{\alpha}) = e^{\kappa \cdot cos(\varphi - \mu)} \cdot e^{-\kappa} \left(\hat{A} - \bar{\alpha} \right) + \bar{\alpha}, \tag{22}$$

where $\hat{A}$ is the maximum value of the beamformer output. In our work we assume that the joint elevation-azimuth distribution can be factored into terms for elevation and azimuth that each follow (21), i.e.,

$$f_{\varphi,\vartheta,\text{UD}}(\varphi, \vartheta, \mu_\varphi, \mu_\vartheta, \kappa_\varphi, \kappa_\vartheta, \bar{\alpha}_\varphi, \bar{\alpha}_\vartheta) = f_{\varphi,\text{UD}}(\varphi, \mu_\varphi, \kappa_\varphi, \bar{\alpha}_\varphi) \cdot f_{\vartheta,\text{UD}}(\vartheta, \mu_\vartheta, \kappa_\vartheta, \bar{\alpha}_\vartheta) \tag{23}$$

Parameters of $\mathbf{K}(\theta_{\text{T/R}})$ in the spatial domain are given by $\theta_{\text{T}} = [\mu_{\varphi,\text{T}}, \mu_{\vartheta,\text{T}}, \kappa_{\varphi,\text{T}}, \kappa_{\vartheta,\text{T}}, \bar{\alpha}_{\varphi,\text{T}}, \bar{\alpha}_{\vartheta,\text{T}}]$ and $\theta_{\text{R}} = [\mu_{\varphi,\text{R}}, \mu_{\vartheta,\text{R}}, \kappa_{\varphi,\text{R}}, \kappa_{\vartheta,\text{R}}, \bar{\alpha}_{\varphi,\text{R}}, \bar{\alpha}_{\vartheta,\text{R}}]$.

Additional discussion on spatial modeling with the Von-Mises distribution is provided in [60], [62], [66].

We extracted DMC spatial-temporal parameters at all measured locations. Statistical distribution fits and corresponding moments for the extracted parameters are provided in Table IV while sample plots of the CDF for parameters such as $\tilde{\alpha}_1$ and $\kappa_{\varphi,\text{T}}$ (both lognormally distributed) confirm a good fit of their logarithmic value to the Gaussian distribution as shown in Figs. 18(a) and 18(b). To further validate the modeling of the DMC, we synthesized the DMC by using (16) - (23). We then generated (i) the power-azimuth-delay-profile (PADP) of the measurement data, which includes both specular and DMC components, (ii) extracted residual components only (from the measurement data) and (ii) the modeled residual at the TX end when taking position 47 as the measurement location. The plots for the PADP are shown in Figs. 16(a) to 16(c). It can be clearly observed from the aforementioned figures that the modeled residual does fit well to the residual obtained from the actual measurement data.

The amount of power that the DMC ($\hat{\eta}_{\text{dmc}}$) contributes to the total channel power is calculated from the $\mathbf{R}_{\text{D}}$ as:

$$\hat{\eta}_{\text{dmc}} = \text{Tr}\{\mathbf{R}_{\text{D}}\}, \tag{24}$$

where $\text{Tr}\{\cdot\}$ is the *Trace* of a matrix. The fractional DMC power $\hat{f}_{\text{dmc}}$, i.e., the percentage the DMC contributes to the total channel power (P_{Tot}) is derived as

$$\hat{f}_{\text{dmc}} = \frac{\hat{\eta}_{\text{dmc}}}{P_{\text{Tot}}} \cdot 100\%. \tag{25}$$

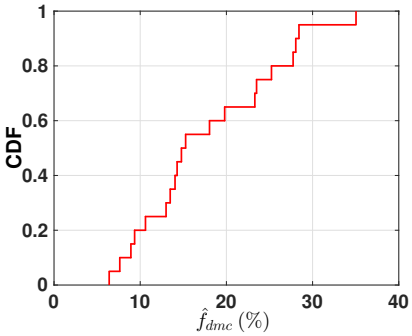

Fig. 17: Empirical CDF of the fraction of power contained in the DMC.

The corresponding CDF of $\hat{f}_{\text{dmc}}$ is provided below in Fig. 17. It can be observed that the average value of $\hat{f}_{\text{dmc}}$ is not too large meaning that the contribution of the DMC is rather moderate in this scenario. Similar effects have also been observed in [62].

V. Model Validation

Verification of the results proceeds in two steps. In a first step, we verify the measurement setup; this has been done in [24] and further confirmed by comparison of the extracted MPCs (and the resulting interactions with the IOs) with a geographical map of the environment as described in Sec. IV-A. In a second step, we verify that the model derived in Sec.

TABLE IV: Extracted parameters.

Parameter	**Notation**	**Values**		
Pathloss coefficient	ξ	3.80		
Pathloss at 1m (reference distance)	P_0 (dB)	23.89		
Bulk shadowing std.	σ (dB)	5.50		
***Intra*-cluster parameters**				
Parameters	EoD	AoD	EoA	AoA
Distribution	Laplacian	Laplacian	Laplacian	Laplacian
cluster angular spread	ESD	ASD	ESA	ASA
Distribution	Lognormal	Lognormal	Lognormal	Lognormal
mean (dB$^\circ$)	0.20	1.09	0.97	1.38
std. (dB$^\circ$)	0.05	0.23	0.24	0.25
Parameter	γ			
Distribution	Lognormal			
mean (dBns)	1.25			
std. (dBns)	0.30			
ray arrival rate (λ) (1/ns)	0.44			
Distribution of the No. of rays per cluster	Exponential			
Average number of rays per cluster	16.0			
Parameter	cluster shadowing gain (SF)			
Distribution	Lognormal			
mean (dB)	0.00			
std. (dB)	7.47			
***Inter*-cluster parameters**				
Parameter	rel. AoD	rel. EoD	rel. EoA	rel. AoA
Distribution	Gaussian	Laplacian	Laplacian	Uniform
Distribution Parameter	mean, std. 6.5°, 14.4°	mean, std. 1.0°, 1.9°	mean, std. 5.1°, 12.7°	min, max -180.0°, 180.0°
Distribution of the No. of cluster	Poisson			
Average number of clusters ($\bar{N}_{\mathrm{k}}$)	3.18			
cluster arrival rate (Λ) (1/ns)	0.015			
cluster decay cnst. (Γ) (ns)	71.23			
cluster polarization				
Pol. Parameters	$\mathrm{XPR}_{\mathrm{HV}}$	$\mathrm{XPR}_{\mathrm{VH}}$		
Distribution	Gaussian	Gaussian		
mean (dB)	6.20	6.10		
std. (dB)	1.59	1.26		
ray polarization				
Pol. Parameters	$\mathrm{XPR}_{\mathrm{HV}}$	$\mathrm{XPR}_{\mathrm{VH}}$		
Distribution	Gaussian	Gaussian		
mean (dB)	$\mathcal{N}(6.20, 1.59)$	$\mathcal{N}(6.10, 1.26)$		
std. (dB)	4.19	4.52		
Cross-correlation				
intra-cluster parameter 1	intra-cluster parameter 2	Coefficient		
ESD	ASD	0.51		
ESA	ASA	0.48		
ESD	ESA	0.13		
ESD	ASA	0.06		
ESA	ASD	0.01		
ASD	ASA	-0.05		
ESD	SF	-0.30		
ASD	SF	-0.33		
ESA	SF	-0.33		
ASA	SF	-0.22		
τ_{rms}	SF	0.03		
τ_{rms}	ESD	0.25		
τ_{rms}	ESA	-0.01		
τ_{rms}	ASD	-0.01		
τ_{rms}	ASA	-0.08		
inter-cluster parameter 1	inter-cluster parameter 2	Coefficient		
rel. AoD	rel. EoD	-0.12		
rel. AoD	rel. EoA	-0.04		
rel. AoD	rel. AoA	0.01		
rel. EoD	rel. EoA	0.10		
rel. EoD	rel. AoA	-0.11		
rel. EoA	rel. AoA	-0.13		
ToA	rel. EoD	0.14		
ToA	rel. AoD	-0.10		
ToA	rel. EoA	-0.12		
ToA	rel. AoA	0.05		
DMC parameters				
Parameter	mean	std.	distribution	
$\bar{\alpha}_1$ (dB)	-117.12	9.09	Gaussian	
$\bar{\beta}_{\mathrm{d}}$	0.15	0.05	Gaussian	
τ_{d} (dBns)	1.40	0.60	Lognormal	
rel. $\mu_{\varphi,\mathrm{T}}(^\circ)$	13.5	9.2	Gaussian	
$\kappa_{\varphi,\mathrm{T}}$ (dB)	15.47	2.76	Lognormal	
$\bar{\alpha}_{\varphi,\mathrm{T}}$	0.93	0.02	Gaussian	
rel. $\mu_{\vartheta,\mathrm{T}}(^\circ)$	5.1	5.3	Gaussian	
$\kappa_{\vartheta,\mathrm{T}}$ (dB)	17.15	6.21	Lognormal	
$\bar{\alpha}_{\vartheta,\mathrm{T}}$	0.94	0.02	Gaussian	
rel. $\mu_{\varphi,\mathrm{R}}(^\circ)$	26.8	23.1	Gaussian	
$\kappa_{\varphi,\mathrm{R}}$ (dB)	9.41	3.72	Lognormal	
$\bar{\alpha}_{\varphi,\mathrm{R}}$	141.60	0.92	Gaussian	
rel. $\mu_{\vartheta,\mathrm{R}}(^\circ)$	14.4	6.6	Gaussian	
$\kappa_{\vartheta,\mathrm{R}}$ (dB)	13.98	4.16	Lognormal	
$\bar{\alpha}_{\vartheta,\mathrm{R}}$	141.63	0.55	Gaussian	

Note that the mean and std. of the rel . EoD are define relative to the geometry of the LOS.
The logarithmic values of the angular spreads (ESD, ASD, ESA, ASA) and delay spread (τ_{rms}) are computed as $\log_{10}(\cdot)$ (dB).
Note that rel. $\mu_{\varphi,\mathrm{T}}(^\circ)$, $\mu_{\vartheta,\mathrm{T}}(^\circ)$, $\mu_{\varphi,\mathrm{R}}(^\circ)$ and $\mu_{\vartheta,\mathrm{R}}(^\circ)$ correspond to the relative (with respect to the geometric LOS) values.

IV reproduces channel characteristics in agreement with the underlying raw measurement data. For this purpose, we use the rms delay and the directional spreads as validation metrics by comparing results obtained from the overall channel model simulation to those obtained directly from the measurement data.

We finally note that these steps are *not* a proof that the model holds for any arbitrary urban environment, but rather that the model correctly reproduces the measurements in our

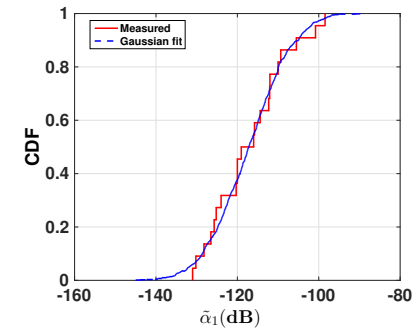

(a)

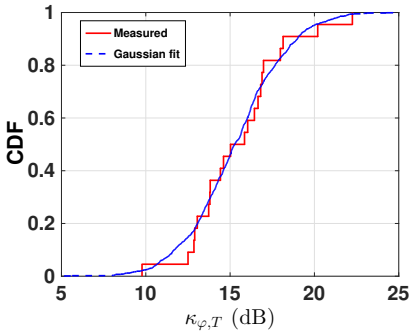

(b)

Fig. 18: Empirical CDF of DMC (a) delay parameter $\tilde{\alpha}_1$ (dB) (b) spatial parameter $\kappa_{\varphi,\mathrm{T}}$ (dB) with corresponding Gaussian fit.

specific measured environment. A comparison of the results[9] obtained in our campaign with those of measurements in different environments is given in Table V.

Generally (from Table V), we find that the qualitative behavior of "standard" channel parameters (angular spreads, τ_{rms}, pathloss coefficient and shadowing gain) extracted in this paper is comparable to the measurements enumerated in Table V as well as to *urban macrocellular models* exisiting in the literature, such as the COST models [32], [68]. It is important to note that the aggregate channel parameters from our work have been used for comparison in Table V and not the *cluster-based* results as this affords us the opportunity to compare with existing models since there is a dearth in *cluster-based* models. Disparity between some parameters could stem from the difference in the environment as well as differences in measurement setup, parameter extraction algorithms, etc.

A. RMS delay spread

The CDF plots of τ_{rms} obtained from raw data and model results are provided in Fig. 19. It is clearly observable that the CDF of the τ_{rms} values derived from the simulation provides a close fit to that derived from the actual measurement data.

[9]To ease the comparison of our results with those in other papers, the angular spreads in Table V have been computed using eq. (6.58) in [53] instead of the Fleury definition [67].

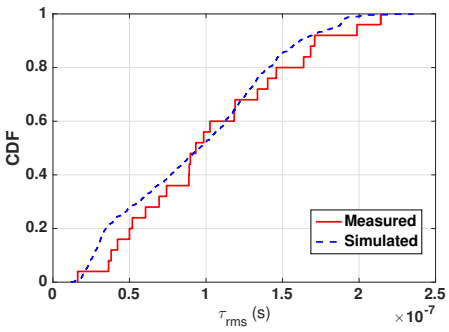

Fig. 19: Empirical CDF of rms-delay spread computed from measurement and corresponding simulated rms-delay spread obtained from the channel model.

B. Directional spread

The directional spread is used to compare the statistical angular properties of the channel model to that of the measurement data. Figs. 20(a) and 20(b) compares DoD direction spread in elevation (σ_{el}) and azimuth (σ_{az}) according to the definition of Fleury [67]. Again simulated channel model results agree quite well with the measurement results, which implies that our channel model is indeed appropriate to reproduce the measured data.

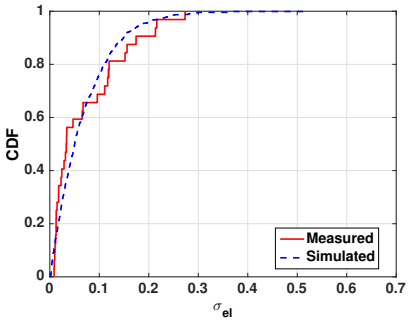

(a)

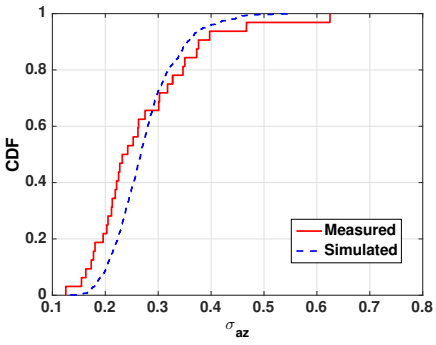

(b)

Fig. 20: Empirical CDF of the (a) DoD σ_{el} (b) DoD σ_{az} computed from measurement data and corresponding simulation values obtained from the model.

TABLE V: Comparing extracted channel parameters from different papers.

Papers	Values	ESD $\log_{10}([^\circ])$	ASD $\log_{10}([^\circ])$	ESA $\log_{10}([^\circ])$	ASA $\log_{10}([^\circ])$	τ_{rms} $\log_{10}([s])$	ξ	χ_σ (dB)	measurement environment, setup, and type of parameters
This paper	mean (dB)	0.52	1.09	1.29	1.83	-6.97	3.80	5.50	• NLOS urban macrocellular European oldtown (mid-rise buildings), Cologne, Germany. • 3D MIMO with 900 element TX array (cylindrical - with synthetic aperture configuration) by 32 element RX array (cylindrical) using an RF switch. • Center frequency: 2.35 GHz, bandwidth: 20 MHz. • High-resolution parameter extraction (RIMAX). • *Cluster-based* modeling. • Provides all parameters for 3D modeling including DMC.
	std. (dB)	0.15	0.23	0.13	0.25	0.36			
Ref. [69]	mean (dB)	0.83	1.05	1.26	1.87	-6.51	N/A	N/A	• LOS and NLOS urban macrocellular and microcelluar environment with modern high-rise buildings, Xian, China. Only results for NLOS shown here. • 3D MIMO with 32 element TX array (dual polarized 8 $\times$ 8 planar) elements by 50 element RX array (arbitrary – *crown-shaped*) using an RF switch. • Center frequency: 2.6 GHz, bandwidth: 35 MHz. • High-resolution parameter extraction algorithm (SAGE). • Models – angular and delay statistics of rays, but not pathloss, shadowing, polarization and DMC. Model is not cluster-based.
	std. (dB)	0.04	0.10	0.16	0.11	0.23			
Ref. [11]	mean (dB)	0.77	1.09	1.17	1.84	-6.44	N/A	N/A	• NLOS urban macrocellular European oldtown (mid-rise buildings), Cologne, Germany. • 3D MIMO with 32 element TX array (cylindrical) by 32 element RX array (cylindrical) using an RF switch. • Center frequency: 2.35 GHz, bandwidth: 20 MHz. • High-resolution parameter extraction (RIMAX). • Models – angular and delay spread statistics of rays, but not pathloss, shadowing, polarization and DMC. Model is not cluster-based.
	std. (dB)	0.27	0.25	0.19	0.15	0.31			
Ref. [16]	mean (dB)	N/A	N/A	1.09	1.85	-6.49	N/A	N/A	• Mostly NLOS urban macrocellular European oldtown (mid-rise buildings), Mulhouse, France. • 3D SIMO with a single element TX antenna by 441 element RX array (21 $\times$ 21 virtual uniform planar configuration). • Center frequency: 2.2 GHz, bandwidth: 62.5 MHz • Beamforming parameter extraction algorithm. • Models – angular spread (at RX), delay spread and polarization of rays, but not angular characteristics at TX, pathloss, shadowing and DMC. Model is not cluster-based.
	std. (dB)	only a single sample result was provided							
Ref. [70]	mean (dB)	N/A	0.33	1.31	1.60	-7.15	N/A	8.30	• LOS and NLOS urban macrocellular European oldtown (mid-rise buildings), Ilmenau, Germany. Only results for NLOS shown here. • 3D MIMO with 16 element TX array (uniform linear configuration) by 48 element RX array (cylindrical) + MIMO-Cube using an RF switch. • Center frequency: 2.53 GHz, bandwidth: 2 $\times$ 45 MHz. • High-resolution parameter extraction (RIMAX). • Describes angular spread (at the RX), delay spread, pathloss and shadowing, but not elevation spread at TX, polarization and DMC. Model is not cluster-based.
	std. (dB)		0.35	0.16	0.21	0.18			

Note that the parameter values from Ref. [16] are from a single sample value (not over an ensemble). Also, the results are from the VV-polarization measurements.

VI. Summary and Conclusion

We conducted a 3D propagation channel measurement campaign in an urban macrocellular NLOS environment using an advanced MIMO antenna array setup. We extracted parameters using RIMAX – a high-resolution parameter extraction algorithm. Our main findings can be summarized as follows:

- The MPCs can be explained by physical propagation routes in the environment.
- MPCs are naturally grouped together into clusters in the propagation environment. A detailed clustering analysis of the propagation channel was provided.
- In line with findings in previous papers, the *intra*-cluster DoD/DoA follows a Laplacian distribution with the angular and delay spread parameters being lognormally distributed and the *inter*-cluster parameters such as EoD and EoA follow Laplacian distribution while AoD and AoA were Gaussian and uniformly distributed respectively. The cluster relative delay is exponentially distributed.
- For the cluster polarization, the cross-polarization ratios (XPR) in dB are Gaussian distributed with mean about 6 dB. The co-polarized values are equal. The XPR of rays in dB are modeled as Gaussian distributed random variable with mean as the cluster XPR value while standard deviation values are 4.2 (XPR_{HV}) and 4.5 dB for XPR_{VH}.
- The pathloss can be modeled as a single-slope power law with pathloss exponent (ξ) 3.8 while the bulk shadowing is zero-mean lognormal distributed with standard deviation of about 5.5 dB for the measured distance range of 200-730 m.
- We provide temporal and spatial parameters for the covariance matrices of the DMC and their statistical distributions. The fractional power of the DMC is about 15% on average. This implies that the DMC does contribute a moderate percentage of power to the propagation channel being studied.
- By using two metrics, rms delay spread and directional spreads, we validated that the model can provide a close fit in the CDF plot between the actual data measurement results and that of the synthetic data generated using our developed channel model. The extracted parameters are (as far as comparable data exist) in reasonable agreement

with the existing literature. For parameters that were measured for the first time in this paper, future measurements will be required to assess their sensitivity to the environment.

Although a single 3D measurement campaign like this cannot provide a complete characterization of the whole "urban macrocellular" environment, we however believe that these results are useful for understanding and simulating 3D urban macrocellular propagation channels. We also note that preliminary results from our measurements were used as an input to the 3GPP standardization of 3D channel models [9].

VII. Acknowledgment

The authors would like to thank Deutsche Telekom for their help in facilitating the measurement campaign. Part of this work was supported by the National Science Foundation under the MRI program.

References

[1] S. Sangodoyin, V. Kristem, C. U. Bas, M. Käske, J. Lee, C. Schneider, G. Sommerkorn, J. Zhang, R. Thomä and A. F. Molisch, "Cluster-based analysis of 3D MIMO channel measurement in an urban environment," in *IEEE Military Communications Conference (MILCOM)*, Oct 2015, pp. 744–749.

[2] I. F. Akyildiz, S. Nie, S. Lin, and M. Chandrasekaran, "5G roadmap: 10 key enabling technologies," *Computer Networks*, vol. 106, no. Supplement C, pp. 17 – 48, Nov 2016.

[3] S. C. Lin and I. F. Akyildiz, "Dynamic base station formation for solving NLOS problem in 5G millimeter-wave communication," in *IEEE INFOCOM 2017 - IEEE Conference on Computer Communications*, May 2017, pp. 1–9.

[4] T. Marzetta, "Noncooperative Cellular Wireless with Unlimited Numbers of Base Station Antennas," *IEEE Transactions on Wireless Communications*, vol. 9, no. 11, pp. 3590–3600, November 2010.

[5] E. G. Larsson, O. Edfors, F. Tufvesson and T. L. Marzetta, "Massive MIMO for next generation wireless systems," *IEEE Communications Magazine*, vol. 52, no. 2, pp. 186–195, February 2014.

[6] Y. Kim, H. Ji, J. Lee, Y. H. Nam, B. L. Ng, I. Tzanidis, Y. Li and J. Zhang, "Full dimension MIMO (FD-MIMO): The next evolution of MIMO in LTE systems," *IEEE Wireless Communications*, vol. 21, no. 3, pp. 92–100, June 2014.

[7] Y. Li, Y. Xm, M. Dong, G. Xu, J. C. Zhang, Y. Kim and J. Lee, "Implementation of full-dimensional MIMO (FD-MIMO) in LTE," in *Asilomar Conference on Signals, Systems and Computers*, Nov 2013, pp. 998–1003.

[8] P. H. Kuo, "A glance at FD-MIMO technologies for LTE," *IEEE Wireless Communications*, vol. 23, no. 1, pp. 2–5, February 2016.

[9] 3GPP TR 25.996, "Spatial channel model for Multiple Input Multiple Output (MIMO) simulations," Tech. Rep. [Online]. Available: http://www.3gpp.org/ftp/Specs/htmlinfo/ 25996.htm

[10] J. Medbo, H. Asplund, J. E. Berg, and N. Jalden, "Directional channel characteristics in elevation and azimuth at an urban macrocell base station," in *2012 6th European Conference on Antennas and Propagation (EUCAP)*, 2012, pp. 428–432.

[11] G. Sommerkorn, M. Käske, C. Schneider, S. Häfner, and R. Thomä, "Full 3D MIMO channel sounding and characterization in an urban macro cell," in *2014 XXXIth URSI General Assembly and Scientific Symposium (URSI GASS)*, Aug 2014, pp. 1–4.

[12] M. Toeltsch, J. Laurila, K. Kalliola, A. F. Molisch, P. Vainikainen, and E. Bonek, "Statistical characterization of urban spatial radio channels," *IEEE Journal on Selected Areas in Communications*, vol. 20, no. 3, pp. 539–549, Apr 2002.

[13] K. Kalliola, H. Laitinen, P. Vainikainen, M. Toeltsch, J. Laurila, and E. Bonek, "3-D double-directional radio channel characterization for urban macrocellular applications," *IEEE Transactions on Antennas and Propagation*, vol. 51, no. 11, pp. 3122–3133, Nov 2003.

[14] J. Fuhl, J. P. Rossi and E. Bonek, "High-resolution 3-D direction-of-arrival determination for urban mobile radio," *IEEE Transactions on Antennas and Propagation*, vol. 45, no. 4, pp. 672–682, Apr 1997.

[15] J. Wang, R. Zhang, W. Duan, S. X. Lu, and L. Cai, "Angular spread measurement and modeling for 3D MIMO in urban macrocellular radio channels," in *2014 IEEE International Conference on Communications Workshops (ICC)*, June 2014, pp. 20–25.

[16] A. Dunand and J. M. Conrat, "Dual-Polarized Spatio-Temporal Characterization in Urban Macrocells at 2 GHz," in *2007 IEEE 66th Vehicular Technology Conference*, Sept 2007, pp. 854–858.

[17] A. O. Kaya and D. Calin, "Modeling Three Dimensional Channel Characteristics in Outdoor-to-Indoor LTE Small Cell Environments," in *MILCOM 2013 - 2013 IEEE Military Communications Conference*, Nov 2013, pp. 933–938.

[18] R. Wang, S. Sangodoyin, A. F. Molisch, J. Zhang, Y. H. Nam, and J. Lee, "Elevation characteristics of outdoor-to-indoor macrocellular propagation channels," in *2014 IEEE 79th Vehicular Technology Conference (VTC Spring)*, May 2014, pp. 1–5.

[19] K. Kitao, T. Imai, K. Saito, and Y. Okumura, "Elevation directional channel properties at BS to evaluate 3D beamforming," in *International Symposium on Intelligent Signal Processing and Communications Systems (ISPACS), 2013*, 2013, pp. 640–644.

[20] B. Mondal, T. A. Thomas, E. Visotsky, F. W. Vook, A. Ghosh, Y. h. Nam, Y. Li, J. Zhang, M. Zhang, Q. Luo, Y. Kakishima and K. Kitao, "3D channel model in 3GPP," *IEEE Communications Magazine*, vol. 53, no. 3, pp. 16–23, March 2015.

[21] R. Zhang, X. Lu, J. Zhao, L. Cai, and J. Wang, "Measurement and Modeling of Angular Spreads of Three-Dimensional Urban Street Radio Channels," *IEEE Transactions on Vehicular Technology*, vol. 66, no. 5, pp. 3555–3570, May 2017.

[22] A. F. Molisch and F. Tufvesson, "Propagation channel models for next-generation wireless communications systems," *IEICE Trans. Commun.*, vol. E97-B, no. 10, pp. 2022–2034, Oct 2014.

[23] A. F. Molisch, *3D Propagation Channels: Modeling and Measurements in F. L. Luo and C. J. Zhang (eds.), "Signal Processing for 5G Algorithms and Implementations"*. John Wiley & Sons, Ltd, 2016, pp. 254–272.

[24] R. S. Thomä, D. Hampicke, A. Richter, G. Sommerkorn, and U. Trautwein, "MIMO vector channel sounder measurement for smart antenna system evaluation," *European Transactions on Telecommunications*, vol. 12, no. 5, pp. 427–438, 2001.

[25] R. S. Thomä, M. Landmann, G. Sommerkorn, and A. Richter, "Multi-dimensional high-resolution channel sounding in mobile radio," in *Proceedings of the 21st IEEE Instrumentation and Measurement Technology Conference (IEEE Cat. No.04CH37510)*, vol. 1, May 2004, pp. 257–262.

[26] R. S. Thomä, D. Hampicke, A. Richter, G. Sommerkorn, A. Schneider, U. Trautwein, and W. Wirnitzer, "Identification of time-variant directional mobile radio channels," *IEEE Transactions on Instrumentation and Measurement*, vol. 49, no. 2, pp. 357–364, Apr 2000.

[27] V. Kristem, S. Sangodoyin, C. U. Bas, M. Käske, J. Lee, C. Schneider, G. Sommerkorn, C. J. Zhang, R. S. Thomä and A. F. Molisch, "3D MIMO Outdoor-to-Indoor Propagation Channel Measurement," *IEEE Transactions on Wireless Communications*, vol. 16, no. 7, pp. 4600–4613, July 2017.

[28] A. Richter, "Estimation of radio channel parameters: Models and algorithms," Ph. D. dissertation, Technische Universität Ilmenau, Ilmenau, Germany, 2005. [Online]. Available: www.db-thueringen.de

[29] J. Laurila, K. Kalliola, M. Toeltsch, K. Hugl, P. Vainikainen, and E. Bonek, "Wideband 3D characterization of mobile radio channels in urban environment," *IEEE Transactions on Antennas and Propagation*, vol. 50, no. 2, pp. 233–243, Feb 2002.

[30] S. Sangodoyin, *et* al, "A Generic Modeling of Cluster Propagation, Classification and Performance Evaluation in 3D MIMO Urban Macrocellular Environment," *to be submitted*.

[31] A. F. Molisch, H. Asplund, R. Heddergott, M. Steinbauer and T. Zwick, "The COST 259 Directional Channel Model-Part I: Overview and Methodology," *IEEE Transactions on Wireless Communications*, vol. 5, no. 12, pp. 3421–3433, December 2006.

[32] H. Asplund, A. Glazunov, A. Molisch, K. Pedersen, and M. Steinbauer, "The COST 259 Directional Channel Model-Part II: Macrocells," *IEEE Transactions on Wireless Communications*, vol. 5, no. 12, pp. 3434–3450, December 2006.

[33] ITU-R Report M.2135, "Guidelines for evaluation of radio interface technologies for IMT-Advanced," 2008, http://www.itu.int/publ/R-REP-M.2135-2008/en.

[34] L. Liu, C. Oestges, J. Poutanen, K. Haneda, P. Vainikainen, F. Quitin, F. Tufvesson, and P. Doncker, "The COST 2100 MIMO channel model," *Wireless Communications, IEEE*, vol. 19, no. 6, pp. 92–99, 2012.

[35] N. Czink, P. Cera, J. Salo, E. Bonek, J. p. Nuutinen, and J. Ylitalo, "A Framework for Automatic Clustering of Parametric MIMO Channel

Data Including Path Powers," in *IEEE Vehicular Technology Conference*, Sept 2006, pp. 1–5.
[36] S. Wyne, N. Czink, J. Karedal, P. Almers, F. Tufvesson and A. F. Molisch, "A Cluster-Based Analysis of Outdoor-to-Indoor Office MIMO Measurements at 5.2 GHz," in *IEEE 64th Vehicular Technology Conference, 2006. VTC-2006 Fall. 2006*, Sept 2006, pp. 1–5.
[37] C. Gustafson, K. Haneda, S. Wyne, and F. Tufvesson, "On mm-Wave Multipath Clustering and Channel Modeling," *IEEE Transactions on Antennas and Propagation*, vol. 62, no. 3, pp. 1445–1455, March 2014.
[38] S. Sangodoyin, V. Kristem, A. F. Molisch, R. He, F. Tufvesson, and H. M. Behairy, "Statistical Modeling of Ultrawideband MIMO Propagation Channel in a Warehouse Environment," *IEEE Transactions on Antennas and Propagation*, vol. 64, no. 9, pp. 4049–4063, Sept 2016.
[39] C. Schneider, M. Bauer, M. Narandzic, W. A. T. Kotterman and R. S. Thomä, "Clustering of MIMO Channel Parameters - Performance Comparison," in *VTC Spring 2009 - IEEE 69th Vehicular Technology Conference*, April 2009, pp. 1–5.
[40] C. C. Chong, C. M. Tan, D. I. Laurenson, S. McLaughlin, M. A. Beach, and A. R. Nix, "A new statistical wideband spatio-temporal channel model for 5 GHz band WLAN systems," *IEEE Journal on Selected Areas in Communications*, vol. 21, no. 2, pp. 139–150, Feb 2003.
[41] K. Yu, Q. Li, D. Cheung and C. Prettie, "On the tap and cluster angular spreads of indoor WLAN channels," in *2004 IEEE 59th Vehicular Technology Conference. VTC 2004-Spring (IEEE Cat. No.04CH37514)*, vol. 1, May 2004, pp. 218–222.
[42] N. Czink, X. Yin, H. Ozcelik, M. Herdin, E. Bonek, and B. H. Fleury, "Cluster Characteristics in a MIMO Indoor Propagation Environment," *IEEE Transactions on Wireless Communications*, vol. 6, no. 4, pp. 1465–1475, April 2007.
[43] A. A. M. Saleh and R. Valenzuela, "A statistical model for indoor multipath propagation," *IEEE Journal on Selected Areas in Communications*, vol. 5, no. 2, pp. 128–137, February 1987.
[44] Q. Spencer, B. Jeffs, M. Jensen, and A. Swindlehurst, "Modeling the statistical time and angle of arrival characteristics of an indoor multipath channel," *IEEE Journal on Selected Areas in Communications*, vol. 18, no. 3, pp. 347–360, March 2000.
[45] C.-C. Chong and S. K. Yong, "A generic statistical-based uwb channel model for high-rise apartments," *IEEE Transactions on Antennas and Propagation*, vol. 53, no. 8, pp. 2389–2399, Aug 2005.
[46] F. J. Massey Jr,, "The Kolmogorov-Smirnov Test for Goodness of Fit," *Journal of the American Statistical Association*, vol. 46, no. 253, pp. 68–78, 1951.
[47] S. Wyne, A. Molisch, P. Almers, G. Eriksson, J. Karedal, and F. Tufvesson, "Outdoor-to-Indoor Office MIMO Measurements and Analysis at 5.2 GHz," *IEEE Transactions on Vehicular Technology*, vol. 57, no. 3, pp. 1374–1386, May 2008.
[48] J. Medbo, M. Riback, H. Asplund, and J. Berg, "MIMO channel characteristics in a small macrocell measured at 5.25 GHz and 200 MHz bandwidth," in *VTC-2005-Fall. 2005 IEEE 62nd Vehicular Technology Conference, 2005.*, vol. 1, Sept 2005, pp. 372–376.
[49] X. Yin, B. Fleury, P. Jourdan, and A. Stucki, "Polarization estimation of individual propagation paths using the SAGE algorithm," in *14th IEEE Proceedings on Personal, Indoor and Mobile Radio Communications (PIMRC) 2003.*, vol. 2, Sept 2003, pp. 1795–1799.
[50] G. Ching, M. Ghoraishi, M. Landmann, N. Lertsirisopon, J. I. Takada, T. Imai, I. Sameda, and H. Sakamoto, "Wideband polarimetric directional propagation channel analysis inside an arched tunnel," *IEEE Transactions on Antennas and Propagation*, vol. 57, no. 3, pp. 760–767, March 2009.
[51] Y. Konishi, L. Materum, J. I. Takada, I. Ida and Y. Oishi, "Cluster polarization behavior of a MIMO system: Measurement, modeling and statistical validation of the correlation of its channel parameters," in *2009 IEEE 20th International Symposium on Personal, Indoor and Mobile Radio Communications*, Sept 2009, pp. 1786–1790.
[52] W. Malik, "Polarimetric characterization of ultrawideband propagation channels," *IEEE Transactions on Antennas and Propagation*, vol. 56, no. 2, pp. 532–539, Feb 2008.
[53] A. F. Molisch, *Wireless Communications*, ser. 2nd ed. Wiley - IEEE. Wiley, 2010.
[54] A. F. Molisch, D. Cassioli, C. C. Chong, S. Emami, A. Fort, B. Kannan, J. Karedal, J. Kunisch, H. G. Schantz, K. Siwiak, and M. Z. Win, "A comprehensive standardized model for ultrawideband propagation channels," *IEEE Transactions on Antennas and Propagation*, vol. 54, no. 11, pp. 3151–3166, Nov 2006.
[55] T. S. Rappaport, G. R. MacCartney, M. K. Samimi and S. Sun, "Wideband Millimeter-Wave Propagation Measurements and Channel Models for Future Wireless Communication System Design," *IEEE Transactions on Communications*, vol. 63, no. 9, pp. 3029–3056, Sept 2015.
[56] S. S. Ghassemzadeh, L. J. Greenstein, A. Kavcic, T. Sveinsson, and V. Tarokh, "UWB indoor path loss model for residential and commercial buildings," in *2003 IEEE 58th Vehicular Technology Conference. VTC 2003-Fall (IEEE Cat. No.03CH37484)*, vol. 5, Oct 2003, pp. 3115–3119.
[57] B. Donlan, S. Venkatesh, V. Bharadwaj, R. Buehrer, and J. A. Tsai, "The ultra-wideband indoor channel," in *IEEE 59th Vehicular Technology Conference (VTC Spring)*, vol. 1, May 2004, pp. 208–212.
[58] J. Poutanen, J. Salmi, K. Haneda, V. Kolmonen, F. Tufvesson, and P. Vainikainen, "Propagation Characteristics of Dense Multipath Components," *IEEE Antennas and Wireless Propagation Letters*, vol. 9, pp. 791–794, 2010.
[59] E. Tanghe, D. Gaillot, M. Lienard, L. Martens, and W. Joseph, "Experimental Analysis of Dense Multipath Components in an Industrial Environment," *IEEE Transactions on Antennas and Propagation*, vol. 62, no. 7, pp. 3797–3805, July 2014.
[60] M. Käske and R. Thomä, "Maximum-likelihood based estimation of angular parameters of Dense-Multipath-Components," in *9th European Conference on Antennas and Propagation (EuCAP)*, May 2015, pp. 1–6.
[61] C. Ribeiro, A. Richter, and V. Koivunen, "Joint Angular-and Delay-Domain MIMO Propagation Parameter Estimation Using Approximate ML Method," *IEEE Transactions on Signal Processing*, vol. 55, no. 10, pp. 4775–4790, Oct 2007.
[62] M. Käske and R. Thomä, "Analysis of angular parameters of dense multipath components in an urban macro-cell scenario," in *Proceedings of the 5th European Conference on Antennas and Propagation (EUCAP)*, April 2011, pp. 3429–3433.
[63] J. Salmi, J. Poutanen, K. Haneda, A. Richter, V. M. Kolmonen, P. Vainikainen, and A. F. Molisch, "Incorporating diffuse scattering in geometry-based stochastic MIMO channel models," in *Proceedings of the Fourth European Conference on Antennas and Propagation*, April 2010, pp. 1–5.
[64] B. N. Mukherjee and S. S. Maiti, "On some properties of positive definite toeplitz matrices and their possible applications," *Linear Algebra and its Applications*, vol. 102, pp. 211 – 240, 1988.
[65] T. Greville, "Toeplitz matrices with toeplitz inverses revisited," *Linear Algebra and its Applications*, vol. 55, pp. 87 – 92, 1983.
[66] M. Käske, M. Landmann, and R. Thomä, "Modelling and synthesis of dense multipath propagation components in the angular domain," in *3rd European Conference on Antennas and Propagation*, March 2009, pp. 2641–2645.
[67] B. H. Fleury, "First- and second-order characterization of direction dispersion and space selectivity in the radio channel," *IEEE Transactions on Information Theory*, vol. 46, no. 6, pp. 2027–2044, Sep 2000.
[68] H. Hofstetter, A. F. Molisch, and N. Czink, "A twin-cluster MIMO channel model," in *First European Conference on Antennas and Propagation (EUCAP)*, Nov 2006, pp. 1–8.
[69] Z. Zhong, X. Yin, X. Li and X. Li, "Extension of ITU IMT-Advanced Channel Models for Elevation Domains and Line-of-Sight Scenarios," in *IEEE 78th Vehicular Technology Conference (VTC Fall)*, Sept 2013, pp. 1–5.
[70] C. Schneider, M. Narandzic, M. Käske, G. Sommerkorn, and R. Thomä, "Large Scale Parameter for the WINNER II Channel Model at 2.53 GHz in Urban Macro Cell," in *IEEE 71st Vehicular Technology Conference (VTC 2010-Spring), 2010*, May 2010, pp. 1–5.

Seun Sangodoyin (S'14) received his B.Sc in Electrical Engineering from Oklahoma State University in May 2007, M.Sc in the same field at the University of Southern California (USC) in 2009, he is currently working toward his Ph.D in Electrical Engineering at the University of Southern California (USC). His research interest includes Millimeter-wave (measurement-based) MIMO channel Modeling and analysis, UWB MIMO Radar, Parameter Estimation, Body Area Networks and Stochastic Dynamical Systems. He has been a student member of IEEE for 5 years.

Vinod Kristem received his Bachelor of Technology from the National Institute of Technology (NIT), Warangal in 2007; Master of Engineering degree in Telecommunications from the Indian Institute of Science, Bangalore, India in 2009; Ph.D. degree in Electrical Engineering from University of Southern California, Los Angeles in 2017. From 2009–2011, he was with Broadcom Corp. He is currently a Research Scientist at Intel Corporation working on next generation WiFi. His research interests include multi-antenna systems, Ultrawideband systems, channel measurements and modeling.

C. Umit Bas received the B.Sc. and M.Sc. degrees in electrical and electronics engineering from Koc University, Turkey, in 2010 and 2012, respectively. He is currently pursuing the Ph.D. degree advised by Dr. Andreas F. Molisch in the Department of Electrical Engineering, University of Southern California, USA. He is also serving as the co-manager of the UltraLab. His research interests include design and construction of real-time channel sounders for millimeter-wave and ultra-wideband communications, and wireless propagation channel measurements and modeling.

Martin Käske received the Diplom-Ingenieur degree in communications engineering from Technische Universität Ilmenau, Germany, in 2008. He is currently working as a Research Assistant at the Electronic Measurement Research Laboratory, at Technische Universität Ilmenau, Germany. His research interests include high-resolution parameter estimation, MIMO channel sounding and radio channel modeling with the focus on vehicle-to-vehicle channels.

Juho Lee is currently a Master (technical VP) with Samsung Electronics, where he is leading the research for standardization of 5G mobile communications and Samsungs standardization activity in 3GPP. He also actively has been working on the research and standardization of 3G and 4G technologies such as WCDMA, HSPA, LTE, LTE-Advanced, and LTE-Advanced Pro since he joined Samsung Electronics in 2000. He was a vice chairman of 3GPP RAN1 from February 2003 to August 2009. He received his Ph.D. degree in electrical engineering from Korea Advanced Institute of Science and Technology (KAIST), Korea, in 2000.

Christain Schneider received the Diploma degree in electrical engineering from the Technische Universität Ilmenau, Ilmenau, Germany, in 2001, where he is currently pursuing the Dr.-Ing. degree with the Institute for Information Technology. His main research interests include wireless multidimensional channel sounding, channel characterization, and analysis, and channel modeling for single and multi-link cases in cellular and vehicular networks at micro and millimeter wave bands. He is also active in research for space-time signal processing, adaptive techniques, and passive coherent localization. He received the Best Paper Award at the European Wireless Conference in 2013 and the European Conference of Antennas and Propagation in 2017.

Gerd Sommerkorn received the Dipl.-Ing. (M.S.E.E.) degree from Technische Universität Ilmenau, Germany, in 1995. From 1995 to 1996, he was a research assistant at the Otto-von-Guericke University of Magdeburg, Germany. At the end of 1996, he rejoined the Technische Universität Ilmenau where he has contributed to several federal German and EU projects. In 2006 the research group of Professor Thomä, of which he is a member, received the research award of the federal state of Thuringia, Germany, in the category "Applied Research" for their work on MIMO Channel Sounding Measurement Systems. His research interests include channel sounding measurements and data analysis for channel modeling.

Charlie Jianzhong Zhang [F] is a VP and head of the Standards and Mobility Innovation Lab of Samsung Research America, where he leads research, prototyping, and standards for 5G and future multimedia networks. From 2009 to 2013, he served as the Vice Chairman of the 3GPP RAN1 working group and led development of LTE and LTE-Advanced technologies such as 3D channel modeling, UL-MIMO, CoMP, Carrier Aggregation for TD-LTE. He received his Ph.D. degree from the University of Wisconsin, Madison.

Reiner Thomä (M'92-SM'99-F'07) received the Dipl.-Ing. (M.S.E.E.), Dr.-Ing. (Ph.D.E.E.), and Dr.-Ing. habilitation degrees in electrical engineering and information technology from Technische Universität Ilmenau (TU Ilmenau), Illmenau, Germany, in 1975, 1983, and 1989, respectively. From 1975 to 1988, he was a Research Associate in the fields of electronic circuits, measure- ment engineering, and digital signal processing with TU Ilmenau. From 1988 to 1990, he was a Research Engineer with the Akademie der Wissenschaften der DDR (Zentrum für Wissenschaftlichen Gerätebau), where he was involved in the field of radio surveillance. In 1991, he spent a sabbatical leave with the University of Erlangen-Nürnberg (Lehrstuhl für Nachrichtentechnik). Since 1992, he has been a Professor of electrical engineering (electronic measurement) with TU Ilmenau, where he was the Director of the Institute of Communications and Measurement Engineering from 1999 to 2005. With his group, he has contributed to several European and German research projects and clusters such as the RESCUE, WINNER, PULSERS, EUWB, NEWCOM, COST 273, 2100, IC 1004, IRACON, EASY-A, and EASY-C. He was the speaker of the German nation-wide DFG-focus Project UKoLOS, Ultrawideband Radio Technologies for Communications, Localization and Sensor Applications (SPP 1202). He became an Advisory Board Member of EU Project mmMAGIC. His research interests include measurement and digital signal processing methods such as correlation and spectral analysis, system identification, sensor arrays, compressive sensing, time-frequency and cyclostationary signal analysis, and their application in mobile radio and radar systems including multidimensional channel sounding, propagation measurement, and parameter estimation, MIMO-, mm-wave-, and ultrawideband radar, measurement-based performance evaluation of MIMO transmission systems including over-the-air testing in virtual electromagnetic environments, passive coherent location, and radar sensor systems for object detection, tracking, and imaging. Dr. Thomä is a member of the URSI (Comm. A), VDE/ITG. Since 1999 he has been serving as the Chair of the IEEE-IM TC-13 on measurement in wireless and telecommunications. In 2007, he received the Thuringian State Research Award for Applied Research both for contributions to high-resolution multidimensional channel sounding. In 2014, he received the Vodafone Innovation Award.

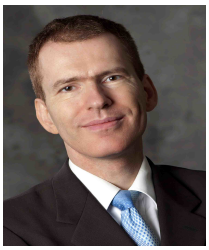

Andreas F. Molisch is the Solomon Golomb Andrew and Erna Viterbi Chair Professor at the University of Southern California. He previously was at TU Vienna, AT&T (Bell) Labs, Lund University, and Mitsubishi Electric Research Labs. His research interest is wireless communications, with emphasis on wireless propagation channels, multi-antenna systems, ultrawideband signaling and localization, novel modulation methods, and caching for wireless content distribution. He is the author of four books, 19 book chapters, more than 220 journal papers, 300 conference papers, as well as 80 patents. He is a Fellow of the National Academy of Inventors, IEEE, AAAS, and IET, as well as Member of the Austrian Academy of Sciences and recipient of numerous awards.